ST-ECF Instrument Science Report WFC3-2009-17

WFC3 SMOV proposal 11552: Calibration of the G141 grism

H. Kuntschner, H. Bushouse, M. Kümmel, J. R. Walsh
October 16, 2009

ABSTRACT

Based on the SMOV observations, the performance of the WFC3 near-IR grism G141 has been assessed. The location of the +1st spectral order relative to the source positions in the direct imaging filters F140W and F160W are determined, field dependent trace and wavelength solutions are derived, and the absolute throughput is quantified. Similar information is derived for higher spectral orders and the -1st order. The trace and wavelength solutions were found to be linear functions, varying smoothly over the field of view. Generally, there is good agreement (<= 1 pixel) with the calibration solutions derived during the ground calibrations in TV2 and TV3.
For the +1st order aperture corrections are provided as a function of wavelength. The cross-dispersion PSF is evaluated and agrees with the design expectations as well as ground calibration measurements.
All calibrations in this ISR are given with respect to source positions derived from F140W images. Source positions obtained from F160W images show only a small systematic offset relative to F140W images of ΔX=0.057±0.003 and ΔY=-0.045± 0.004.
The +1st order of the G141 grism shows a mean dispersion of 46.5 Å/pixel with a resolving power of R~120 at 13000 Å. The throughput of HST + WFC3 G141 peaks at 14350 Å with 47.8% and is above 10% between 10800 and 16900 Å.

1. Introduction

The Wide Field Camera 3 (WFC3) is fitted with three grisms for slitless spectroscopy. In the UVIS channel there is one grism, G280, for the near-UV to visible range (200 - 400nm). The NIR channel has two grisms, G102 and G141, for the shorter (800 - 1150nm) and longer NIR wavelengths (1100-1700nm), respectively. The results from ground calibration efforts, including trace, wavelength, flat-field, throughput and aperture correction calibrations are summarized in Kuntschner et al. (2008a,b) and Kuntschner et al. (2009). This report presents the first in-orbit calibrations for the G141 grism derived from SMOV and selected Cycle 17 calibration observations.

2. Observations

The calibrations presented in this report are based on the SMOV program 11552 (PI: Bushouse), which comprises observations of the HST primary flux standard star GD153, and the wavelength calibrator planetary nebula HB12 (= PN G111.8-02.8) at several positions over the field-of-view (hereafter FoV). Furthermore, we made use of the Cycle 17 calibration program 11937 (PI: Bushouse), which comprises observations of the wavelength calibrator PN Vy2-2 over 9 different field positions. A summary of the pointing locations for all observations is given in Figure 1.

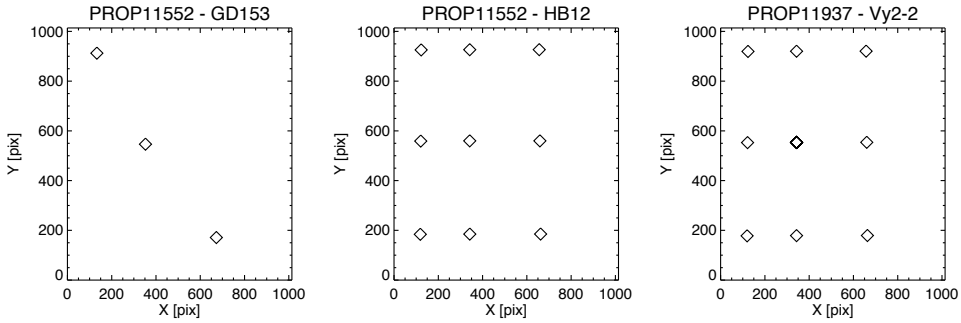

Figure 1: Distribution of target positions as seen on the F140W images for the SMOV proposal 11552 (GD153 and HB12) as well as Cycle 17 calibration proposal 11937 (Vy2-2).

For each position one or more G141 grism exposures were acquired. A detailed listing of all exposures used in this report is given in the Appendix.

3. Analysis

In this section we describe the analysis of the calibration data obtained for the G141 grism in proposals 11552 and 11937 yielding calibrations for the trace, the wavelength solution and the absolute throughput. Furthermore, we investigate offsets between the filters F140W and F160W. If not noted otherwise, analysis was carried out on fully processed images (i.e. “flt” files). The files were produced with the calwf3 pipeline, which carries out the basic data reductions including the following tasks:

- Flag known bad pixels in the data quality (DQ) array
- Subtract bias drifts determined from the reference pixels
- Identify pixels in the initial ("zeroth") read that contain detectable source signal
- Subtract the zeroth read
- Calculate a noise model for each pixel and record in the error (ERR) array
- Subtract dark image
- Correct for photometric non-linearity
- Convert the data to signal rates (in DN per second)
- Perform "up-the-ramp" fitting and cosmic-ray rejection
- Perform flat-fielding and apply gain calibration (to electrons per second)

The grism images are not flat-fielded with the normal procedure since for grism spectroscopy a given pixel can receive any wavelength for which the combination of camera and grism shows throughput. In our analysis we employ a special flat-field procedure where for each extracted pixel a wavelength dependent flat-field is applied; therefore calwf3 only applies the gain calibration to grism images. The grism flat-field information was determined during ground calibration and is stored in a flat-field cube (see Kuntschner et al 2008b).

In Figure 2 we show a typical direct image – G141 grism image pair by using observations of the flux standard star GD153.

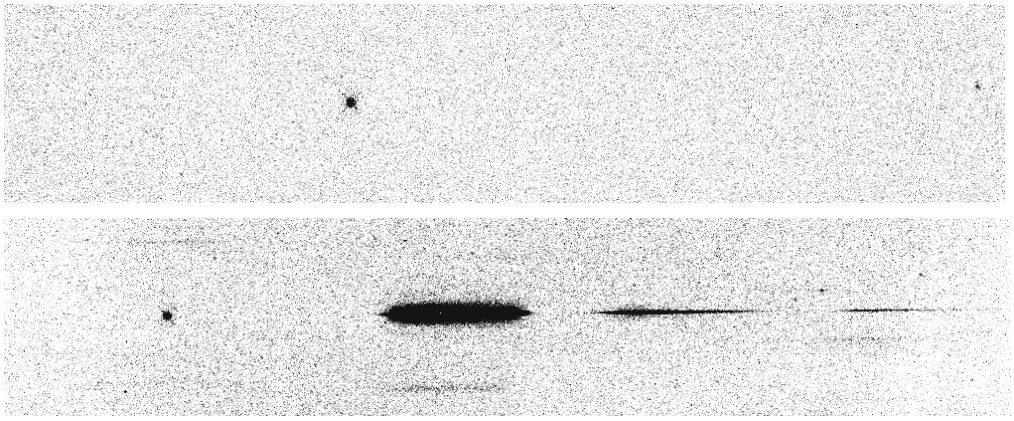

Figure 2: Example of a typical direct image – grism image pair for the G141 grism. The top panel shows a F140W image (iab904meq_flt.fits) of the flux standard GD153 and the bottom panel shows a G141 grism exposure (iab904mgq_flt.fits) for the same region on the sky. The point like source on the left-hand side of the grism image is the zeroth order spectrum; the $+1^{st}$, $+2^{nd}$ and $+3^{rd}$ orders follow to the right. Faint traces of $+1^{st}$ orders from other sources in the field of view are visible in the grism image. For each image we show the full extent of the detector in the x-direction and about 200 pixels in the y-direction.

3.1. Trace calibration

In order to establish a good in-orbit trace calibration, we utilize the G141 grism exposures of the PN HB12. For the trace calibration, we are not interested in the primary target itself but in the other point sources around the primary target. This field (galactic latitude: -02.8498 degrees) comprises a relatively good compromise between field coverage + object density and thus avoiding too much spectral overlap between different sources in the FoV (see Figure 2). The ST-ECF aXe software package for the reduction of slitless spectroscopy data treats the spectral traces and wavelength solutions defined with respect to the position of the source in the direct image. The centroids of all sources above a given threshold in the F140W images (X_{ref}, Y_{ref}) were determined with SExtractor (Bertin &Arnouts, 1996). These positions were assumed not to change between the observations of each direct image grism pair. The spectra of all sources were traced as a function of $\Delta X = X - X_{ref}$ in the detector X-direction by measuring the centroids of 7-10 pixel wide bins, using custom-written IDL programs. We found the traces of all orders (excluding the zeroth order) to be well fit by straight lines with standard deviations of $\leq$ 0.1 pixels. The trace definitions are of the form $(Y - Y_{ref}) = DYDX\_0 + DYDX\_1 * \Delta X$, where DYDX_0 and DYDX_1 are field dependent and given in the usual format used by the ST-ECF aXe reduction package, e.g., DYDX_1 = a0

$+a1*X_{ref} + a2*Y_{ref} + \ldots$ (see also the aXe manual[1] for more details).

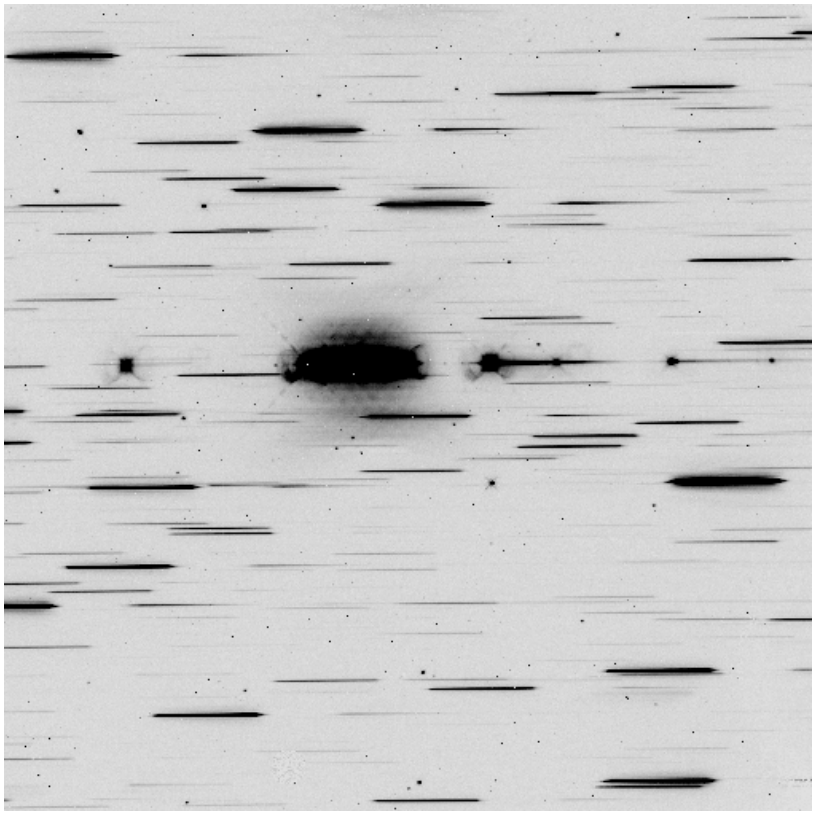

Figure 2: Image of the G141 grism exposure (iab908s4q_flt.fits). The primary target HB12 is located in the centre. Most of the other prominent spectra are first orders of different (stellar) objects in the FoV used for the trace calibration.

The final, field dependent trace solution for the $+1^{st}$ order of the G141 grism was derived from 162 different traces covering semi-uniformly the FOV. A graphical representation of the measured offsets and slopes as a function of X_{ref} and Y_{ref} positions is given in Figure 3. The offset shows a marked trend with Y_{ref} position while the slope shows a more complex dependence on X_{ref} and Y_{ref}. The offset is well represented with a field dependent fit using only a linear function (rms = 0.08 pixel), while the slope required a fit with quadratic terms (rms = 0.0006). The in-orbit calibrations show reasonably good agreement with the ground calibrations obtained in TV2 and TV3 with differences of ~0.3 pixel in the offset and good

[1] http://www.stecf.org/software/slitless_software/axe/

agreement for the slope. The results of our field dependent fits are given in Table 1 and are also shown in Figure 3.

For the -1st, +2nd and +3rd orders a similar procedure was carried out, however, due to the reduced field coverage for these orders the field dependent fits were more restricted and the trace prediction accuracy is reduced. Results are summarized in Table 1. For the 0th order we adopt the trace determined in the ground calibrations. The +4th order spectra are visible for sources located at $X_{ref} \leq 270$, however, this order is not analysed as part of this ISR and will be determined at a later stage.

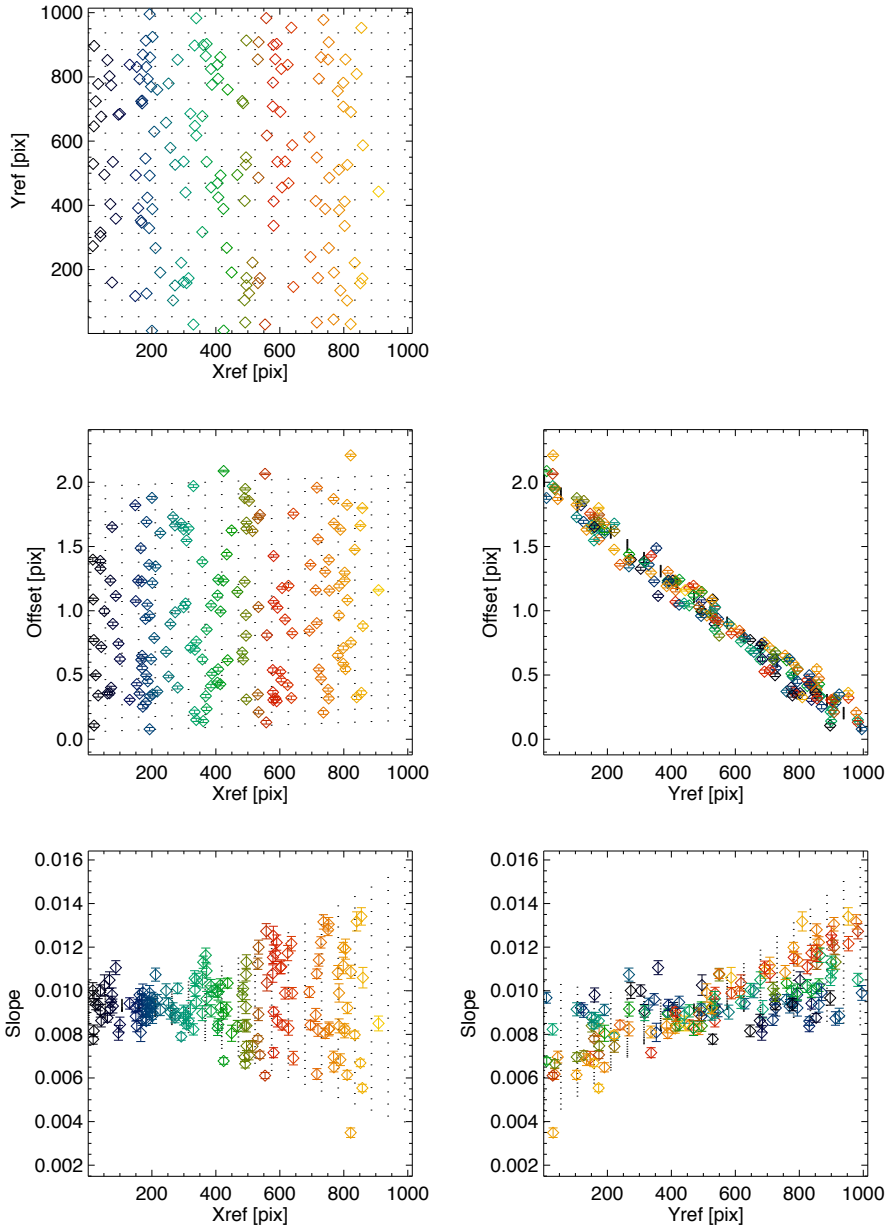

Figure 3: The trace fits for the G141 1st order spectra are shown as a function of X_{ref} and Y_{ref} position (diamond symbols). A total of 162 different source positions are used covering well the field-of-view (top left panel). The final field-dependent trace solution fit (see also Table 1) is shown as the grid of black dots.

Table 1: Field dependent trace descriptions for G141. Where available errors are given below the values

Term	a0	a1(X)	a2(X)	a3(X^2)	a4(X*Y)	a5(Y^2)
			+1st order			
DYDX_A_0	1.96882E+00	9.09159E-05	-1.93260E-03	-	-	-
error	8.09111E-02	3.57223E-06	3.12042E-06	-	-	-
DYDX_A_1	1.04275E-02	-7.96978E-06	-2.49607E-06	1.45963E-09	1.39757E-08	4.84940E-10
error	5.94731E-04	4.34517E-07	3.57986E-07	3.87141E-10	3.29421E-10	3.08712E-10
			0th order			
DYDX_B_0	6.58628E-01	1.58398E-04	-1.62512E-03	-	-	-
DYDX_B_1	0.0	-	-	-	-	-
XOFF_B	-1.92240E+02	-2.31440E-03	1.11089E-02	-	-	-
YOFF_B	0.0	-	-	-	-	-
			+2nd order			
DYDX_C_0	2.26624E+00	-1.78192E-04	-2.71785E-03	-	-	-
error	4.83732E-01	1.92052E-05	1.34415E-05	-	-	-
DYDX_C_1	5.39806E-03	2.78779E-06	4.84354E-06	-	-	-
error	1.57094E-03	3.53707E-07	2.47603E-07	-	-	-
			+3rd order			
DYDX_D_0	3.05905E+00	0.0	-5.51206E-03	-	-	-
error	5.02518E-01	-	2.65696E-05	-	-	-
DYDX_D_1	5.65708E-03	0.0	6.87491E-06	-	-	-
error	1.22990E-03	-	3.43741E-07	-	-	-
			-1st order			
DYDX_E_0	4.19045E+00	0.0	-8.53483E-03	-	-	-
error	1.11680E+00	-	1.30599E-04	-	-	-
DYDX_E_1	1.39687E-02	0.0	-1.77629E-05	-	-	-
error	2.44552E-03	-	3.05845E-06	-	-	-

Notes: The 0th order trace solutions are taken from the ground calibrations.

3.2. Position dependence on filter

The trace and wavelength calibrations reported in this ISR are based on the source positions measured from the standard filter F140W. An alternative filter for the G141 grism would be F160W. If the F160W filter would introduce a shift in source pixel positions with respect to the F140W filter, the trace and wavelength calibrations are directly affected. For the WFC3 G102 grism and its associated filters F098M and F105W, we detected shifts of up to 0.3 pixel (see Kuntschner et al. 2009). We tested for these potential shifts by using the imaging of Proposal 11937 (PN Vy2-2). For each pair of F140W and F160W images taken at the same

POSTARGS, we ran Sextractor and matched the source positions. In total there are 9 image pairs, which yielded 2492 matched object positions after some robust cleaning had been applied.

The resulting mean offsets were derived with a biweight mean estimator (IDL biweight_mean.pro) and are given in Table 2. The analysis showed little evidence for a field-position dependence of the shifts as can be seen from Figure 4. Since the shifts are smaller than 1/10 of a pixels it will generally not be required to apply any offsets.

Table 2: Source position offsets between F140W and F160W

	X offset [pixel]	**Y offset [pixel]**
F140W – F160W	**0.057±0.003**	**-0.045±0.004**

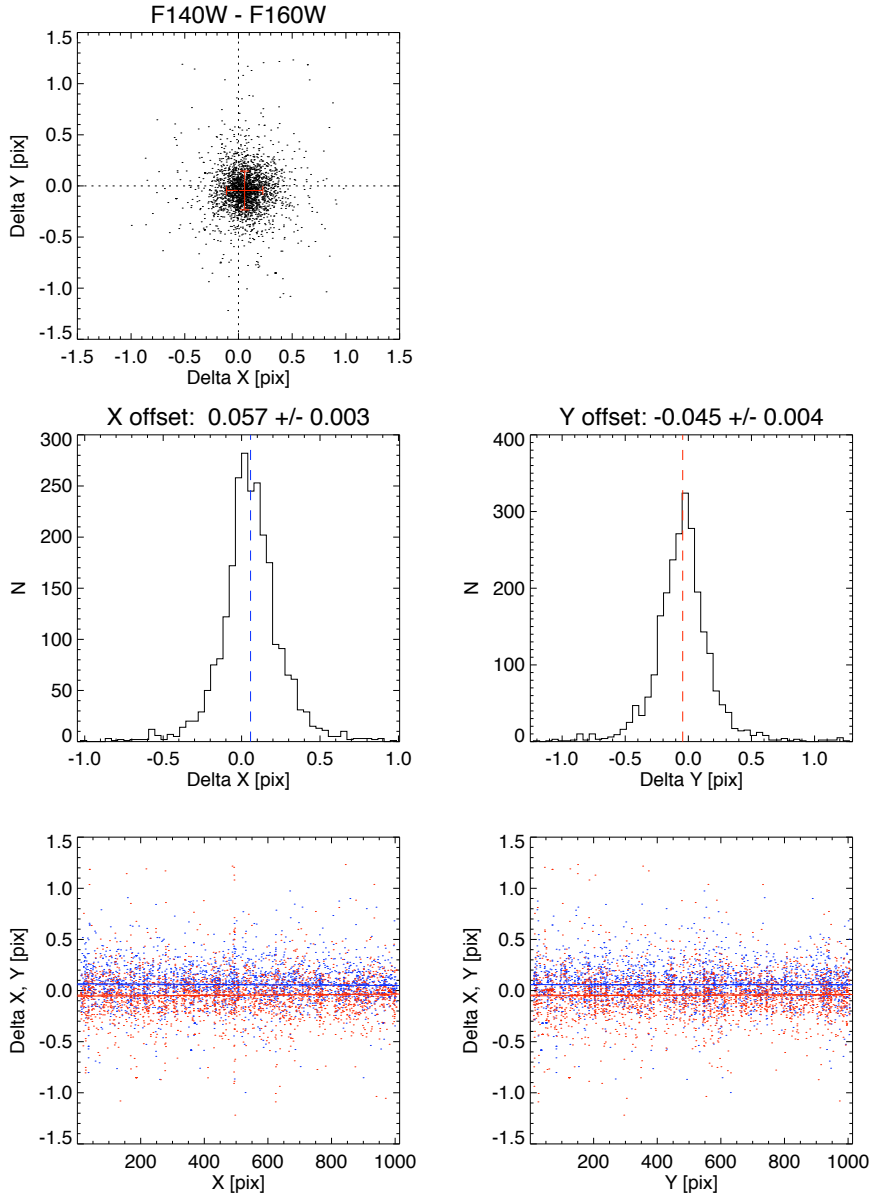

Figure 4: Source position shifts between the filters F140W and F160W. A total of 2492 sources were matched in the direct imaging of Proposal 11937. Individual offsets and the mean are shown in the top panel. Histograms versus x and y-axis are shown in the middle panels whereas potential offset dependence with X and Y position is explored in the bottom panels. Solid lines show a robust linear fit, while the dashed lines indicate the mean shift in x (blue) and y (red).

3.3. Wavelength solutions

In order to establish the in-orbit wavelength calibration, the PN HB12 was observed during SMOV (Proposal 11552). Despite the extended nature of the object, the central pixels of the source saturate even in the first read of the direct image, which makes it difficult to determine an accurate source position. The PN Vy2-2 was observed as a wavelength calibrator as part of the Cycle 17 calibration program (Proposal 11937). This PN is somewhat fainter and accurate positions of the source could be derived from the direct imaging. However, also here the first read is slightly saturated and the final positions were derived from the zeroth read using the "*_raw.fits" files.

For wavelength calibration one would ideally want point sources with clearly identifiable emission lines over the wavelength range and at the resolution of the grism. While bright, nearby PNs do show a reasonably good distribution of emission lines, they are slightly extended at the spatial resolution of the WFC3 IR camera. Since the PNs Vy2-2 and HB12 have already been used for NICMOS grism calibration (see Pirzkal et al. 2009) and they offer a reasonable balance between brightness, number of emission lines and wavelength coverage, we opted for using those targets in the first wavelength calibrations of the WFC3 IR grisms. Future calibration programs may consider the use of e.g., WR stars or M-dwarfs.

Using the trace calibration described in Section 3.1 we extracted the spectra of Vy2-2 at all nine field positions with the help of the aXe software. In this extraction a special configuration file was used which provided spectra with counts versus pixel number along the x-axis. For the G141 grism ($+1^{st}$ order) a total of 7 emission features could be identified and used to establish the wavelength solution (see Table 3). Prior to the fitting, the radial velocity of -71 km/s for Vy2-2 and an air to vacuum conversion was applied to the tabulated wavelength of the emission lines (see Table 3). The ground calibration efforts suggested that a linear wavelength solution is a good representation of the true wavelength solution for this grism (Kuntschner et al. 2008a, b). Therefore we established for each spatial position a linear wavelength solution (see Figure 5) where fits give a typical rms scatter of 0.2-0.3 pixel (see Figure 5). The resulting wavelength solution shows typical errors of 9 Å for the zeropoint and 0.07 Å/pixel for the dispersion (~46.5 Å/pixel). Sometimes the emission lines are affected by e.g., cosmic ray hits, hot/dead pixels etc. and thus good emission line centroids could not be established. Therefore we used a 3-sigma rejection iteration for each linear fit to remove outliers.

Table 3: Rest air wavelength of emission features fitted to Vy2-2

Name	Wavelength [Å]
He I	10830.3
He I	11969.1[2]
He I	12784.9 [2]
H B13	16109.3
H B12	16407.2
H B11	16806.5
H B10	17362.1

[2] A ground based spectrum of Vy2-2 (Hora et al. 1999) suggests that at the spectral resolution of the G141 grism the effective peak wavelength requires adjustments of -10.4 and +34.6 Å, for the He I emission lines at 11969.1 and 12784.9 Å. Before determining the dispersion solution these adjustments were applied.

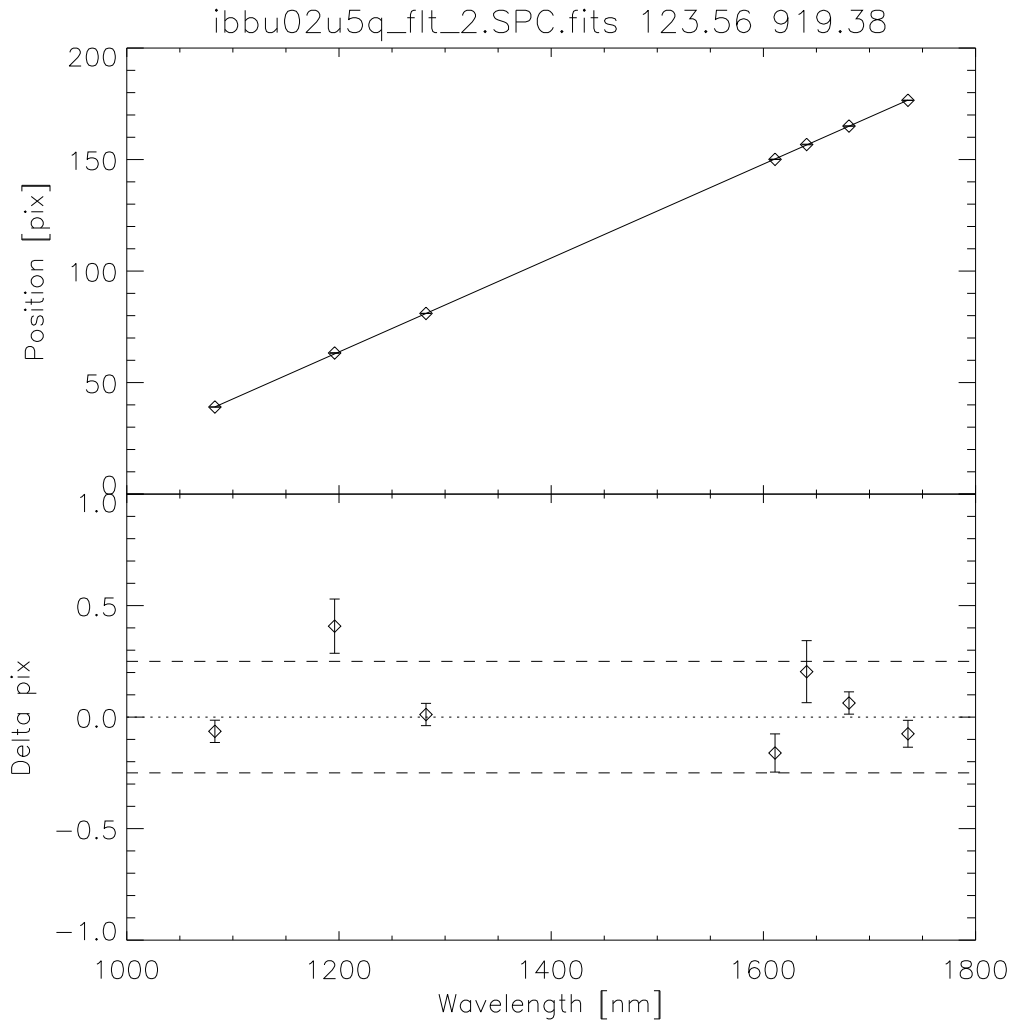

Figure 5: Linear fit for the wavelength solution of the G141 grism. The example shows a fit for one pointing (X_{ref}=123.56, Y_{ref}=919.38). The top plot shows the fit whereas the bottom panel shows the deviations from the linear fit; the dashed lines indicate ±0.25 pixel deviation from the fit.

A similar procedure was used to establish wavelength solutions for the +2nd, +3rd and -1st orders of the G141 grism. Due to the finite detector size and therefore reduced wavelength coverage for the higher orders a reduced number of emission lines was used in these fits. The average dispersion per pixel in the higher orders is higher by the approximate ratio of the orders. It is 23.6, 15.7 and -48.7 Å/pix for the +2nd, +3rd, and -1st order, respectively.

Following the methodology used for the trace calibrations we established field

dependent (2-dimensional) fits for the wavelength solution (see Figure 6 and Table 5). The fit shows a marked trend of the wavelength zeropoint with X_{ref} position. A trend with Y_{ref} position was not significant and thus set to 0.0. The zeropoint measurements show an rms scatter of about 8 Å with respect to the fit. For the dispersion we find a marked trend with Y_{ref} position and a much weaker, quadratic trend with X_{ref} positions. The dispersion varies approximately from 45.0 to 47.5 Å/pixel across the full field of view. The measurements show a rms scatter of 0.06 Å/pixel with respect to the fit.

Compared to the ground calibration measurements in TV3 we find a significant change as detailed in Table 4 for a source position at X_{ref}=340 and Y_{ref}=550. However, over most of the wavelength range of the G141 grism the differences are less than one pixel in dispersion direction. The differences are possibly caused by gravity release.

Table 4: Wavelength solution comparison between TV3 and SMOV for a source at X_{ref}=340 and Y_{ref}=550.

	Zeropoint [Å]	Dispersion [Å/pixel]
TV3	8953.0	46.792
SMOV	8986.1	46.517

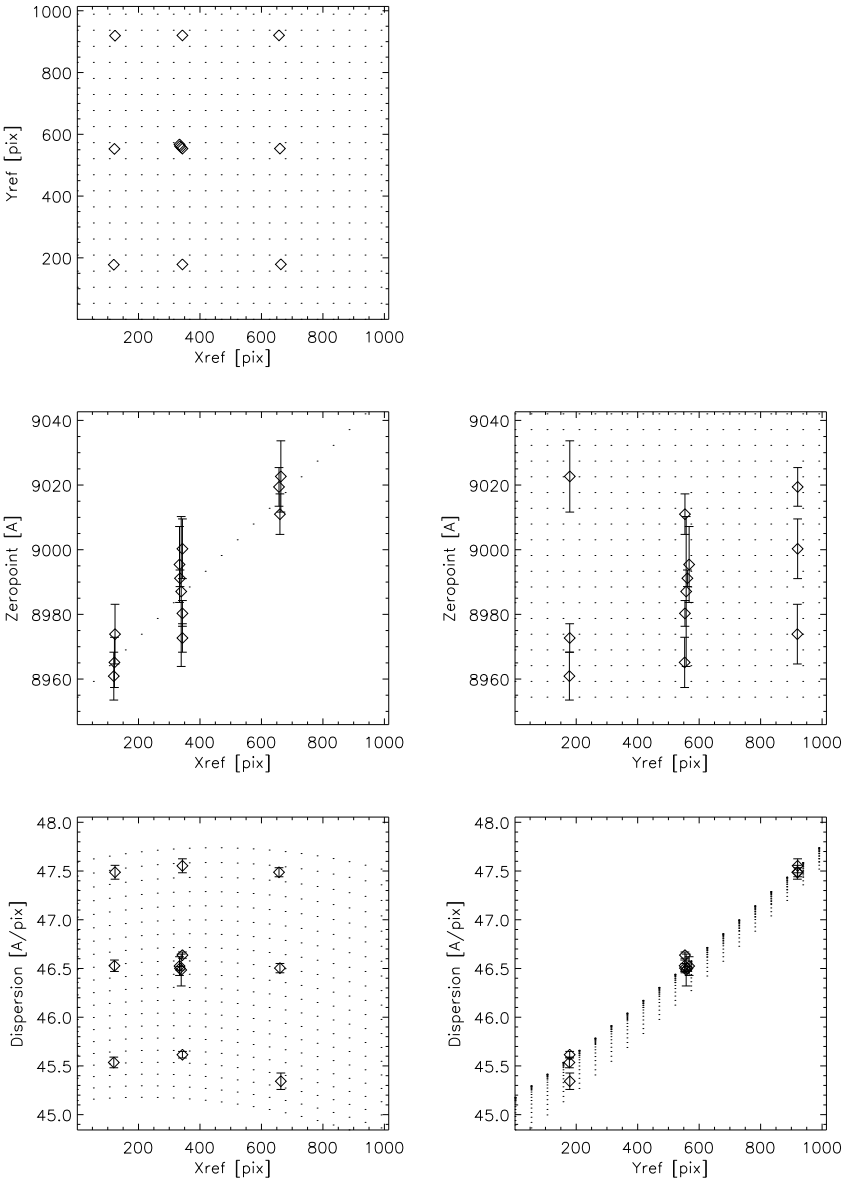

Figure 6: The wavelength solution for the G141 1st order spectra is shown as a function of X_{ref} and Y_{ref} position (diamond symbols). The final field-dependent wavelength solution (see also Table 5) is shown as the grid of black dots.

Table 5: Field dependent wavelength solution for G141. Where available errors are given below the values

Term	a0	a1(X)	a2(Y)	a3(X^2)	a4(X*Y)	
			+1st order			
DLDP_A_0	8.95431E+03	9.35925E-02	0.0	-	-	-
error	8.14876E+00	1.09748E-02	-	-	-	-
DLDP_A_1	4.51423E+01	3.17239E-04	2.17055E-03	-7.42504E-07	3.48639E-07	3.09213E-07
error	6.26774E-02	3.98039E-04	2.31850E-04	4.45730E-07	3.20519E-07	2.16386E-07
			0thorder			
DLDP_B_0	1.28397E+04	-	-	-	-	-
DLDP_B_1	2.32405E+03	-	-	-	-	-
			+2nd order			
DLDP_C_0	4.48233E+03	7.61896E-02	-2.70153E-03	-	-	-
error	2.79017E+00	2.26239E-02	1.01228E-02	-	-	-
DLDP_C_1	2.28943E+01	-1.81224E-04	1.40766E-03	-	-	-
error	9.95420E-03	5.51487E-05	2.95185E-05	-	-	-
			+3rd order			
DLDP_D_0	3.00187E+03	1.04205E-01	-1.18134E-03	-	-	-
error	6.60071E+00	8.33292E-02	3.99081E-02	-	-	-
DLDP_D_1	1.52552E+01	-2.08555E-04	9.55645E-04	-	-	-
error	1.23680E-02	1.41001E-04	6.74659E-05	-	-	-
			-1st order			
DLDP_E_0	-9.37152E+03	0.0	1.71214E-01	-	-	-
error	2.56600E+00	-	1.00445E-01	-	-	-
DLDP_E_1	-4.68834E+01	0.0	-2.48997E-03	-	-	-
error	1.22200E-02	-	2.29997E-04	-	-	-

In Figure 7 we show the individual emission lines of Vy2-2 after the flux calibration (see Section 3.3) and our field-dependent trace and wavelength solutions have been applied to the data. Overall, the field dependent calibrations provide a satisfactory result.

A further test of our in-orbit wavelength calibrations was performed by making use of the flux standard star GD153 (see also Section 3.3). The G141 grism covers the wavelength of the prominent Hydrogen Paschen series lines H P5 (12818.1 nm), which is clearly seen in the white dwarf GD153. Using the direct pixel fitting code ppxf (Cappellari & Emsellem 2004) we fit a model spectrum of GD153 (CALSPEC library; gd153_mod_005.fits) to the observed spectrum. The ppxf IDL routine involves the logarithmic rebinning of the spectrum and we chose a value of 1085 km/s/pixel. We measure a relative velocity between our observations and the model spectrum of 1±70 km/s, which corresponds to 0.0±0.06 velocity pixels. The above numbers indicate an accuracy of the wavelength zeropoint of <0.25 pixel. From the fitting procedure, we can also provide a rough estimate of the spectral

resolution at the wavelength of the two Paschen lines and obtain R=116±11 at 13000 nm or a FWHM of 112±11 Å. This is lower than what would be inferred from the cross-dispersion profile (see Figure 13), however, it is broadly in agreement with the 2 * pixel FWHM (2*46.5=93 Å).

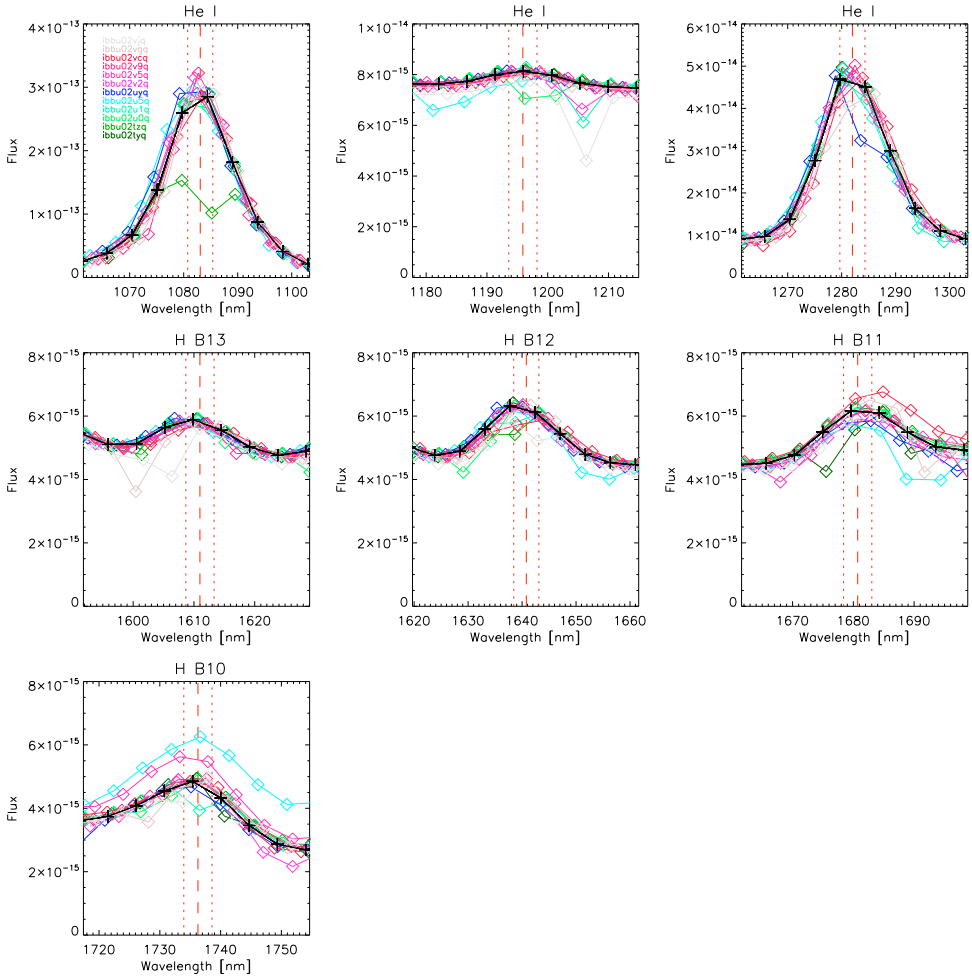

Figure 7: Selected emission lines in the spectra of Vy2-2. The aXe software was used to extract the spectra utilizing our field-dependent trace and wavelength solutions established in Section 3.1 and 3.2. Shown in color are the 12 individual spectra covering 9 spatial pointings (see also Figure 1). The 4 central spectra were combined and are shown in black. The color-coding is given in the top left panel. For each panel and emission line we give the identification of the lines in the title and the central wavelength and ± 0.5 pixel offsets are given as vertical red lines. The central pixels of the He I line (top left panel) in one spectrum (green, ibbu02tzq_flt.fits) are affected by bad detector pixels and therefore the line appears to have a dip at the center.

3.4. Throughput measurements

Using the trace and wavelength solutions derived in the previous sections, the spectra of the flux standard star GD153 observed in Proposal 11552 were extracted. Note, that we make use of our own flat-field calibrations for the G141 grism, which significantly improve the quality of the spectra. There were four, slightly dithered, G141 exposures taken near the central position of the FoV. A further two exposures cover the top left and bottom right corners of the FoV (see Figure 1 and Table A1). For the flux calibration we combine the $+1^{st}$ order of the four central exposures into a single spectrum with the help of the spectral drizzle option in the aXe software (aXedrizzle). This spectrum is used to establish the flux calibration for the G141 grism.

Firstly, the spectrum was converted to units of [e^- / Å / sec] and divided by a smoothed version of the model spectrum taken from the HST CALSPEC library (gd153_mod_005.fits). Smoothing in a sliding 7 pixel window provides the final sensitivity function. The error is evaluated by taking the standard deviation of the four individual sensitivity curves from the central pointings at each wavelength bin and imposing a minimum error of 1%. Using this new sensitivity curve, Figure 8 shows (from the top) the aXe-extracted spectra in electrons per second per pixel, in flux units and the ratio of the observed flux over the model spectrum versus wavelength. In the top plot of Figure 8, significant variations between spectra can be seen since the spectral dispersion (Å/pixel) changes as a function of position within the field-of-view. The overall agreement between the fully calibrated standard star spectra (middle plot) is good for the wavelength range 1050 to 1700 nm. We note, that the two spectra which show up to 4-5% less flux are the ones located at the upper left and lower right positions of the FoV. This is clear evidence for a large-scale illumination variation which still requires correction in the grism flat-field cubes. Observations of the flux standard star GD71 in the Cycle 17 calibration program cover 9 pointings over the FoV and will enable such corrections.

Sensitivity curves were also derived for the 0^{th}, $+2^{nd}$, $+3^{rd}$ and -1^{st} orders. For the $+2^{nd}$ and $+3^{rd}$ orders we combined the 4 central exposures, whereas for the -1^{st} order only one exposure was available. In Figure 9 we summarize the results for all sensitivity curves. Compared to the TV3 results we find up to 10% more throughput in the $+1^{st}$ order. The TV3 results are shown as green lines in Figure 9.

The peak throughput of HST + WFC3 G141 is 47.8% at 1435 nm while it is >10% over the wavelength range 1080 to 1690 nm.

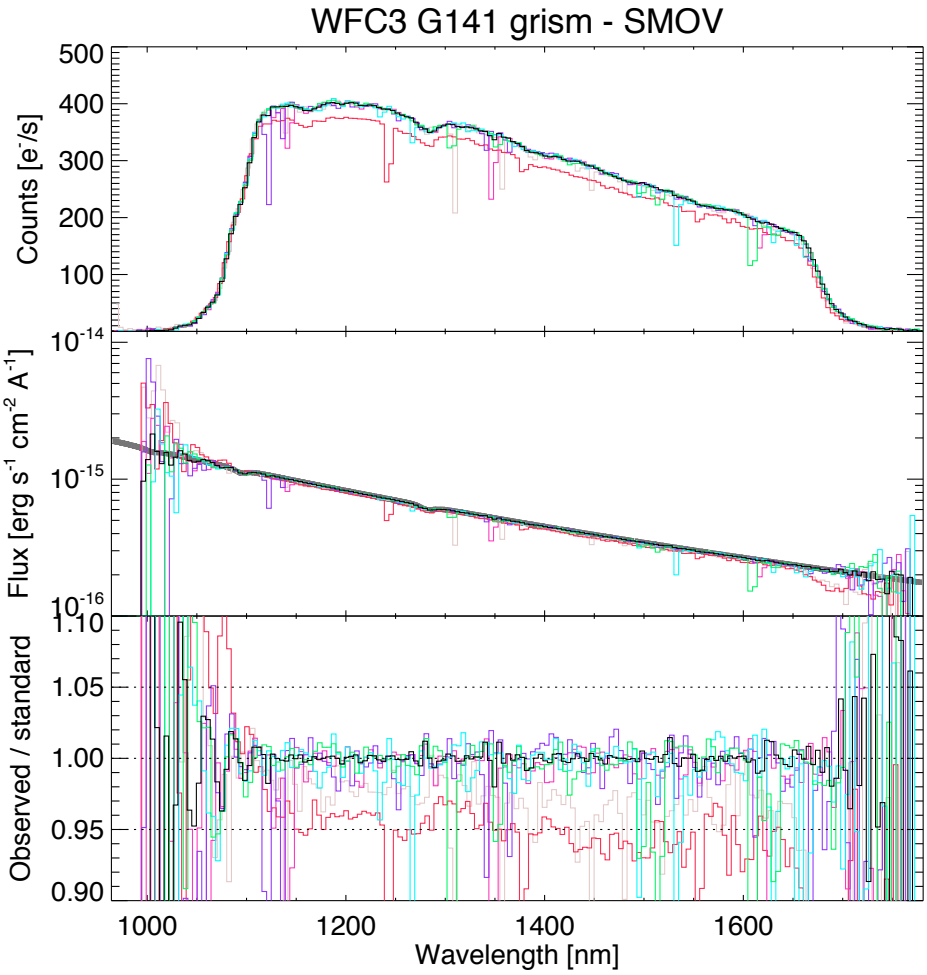

Figure 8: The aXe extracted 1-dimensional spectra of the standard star GD153 in units of electrons per second per pixel, fully calibrated flux units and the ratio of the observed flux over the model spectrum versus wavelength (from top to bottom). Observations obtained at different field positions are colored, and the combined (aXedrizzle) central spectrum is shown in black. In the individually extracted spectra there are a number of prominent wavelength steps, which show too low flux. These points are caused by pixels, which are flagged in the original flt files. The aXedrizzle spectrum corrects for these effects and thus does not show any deviant wavelength steps.

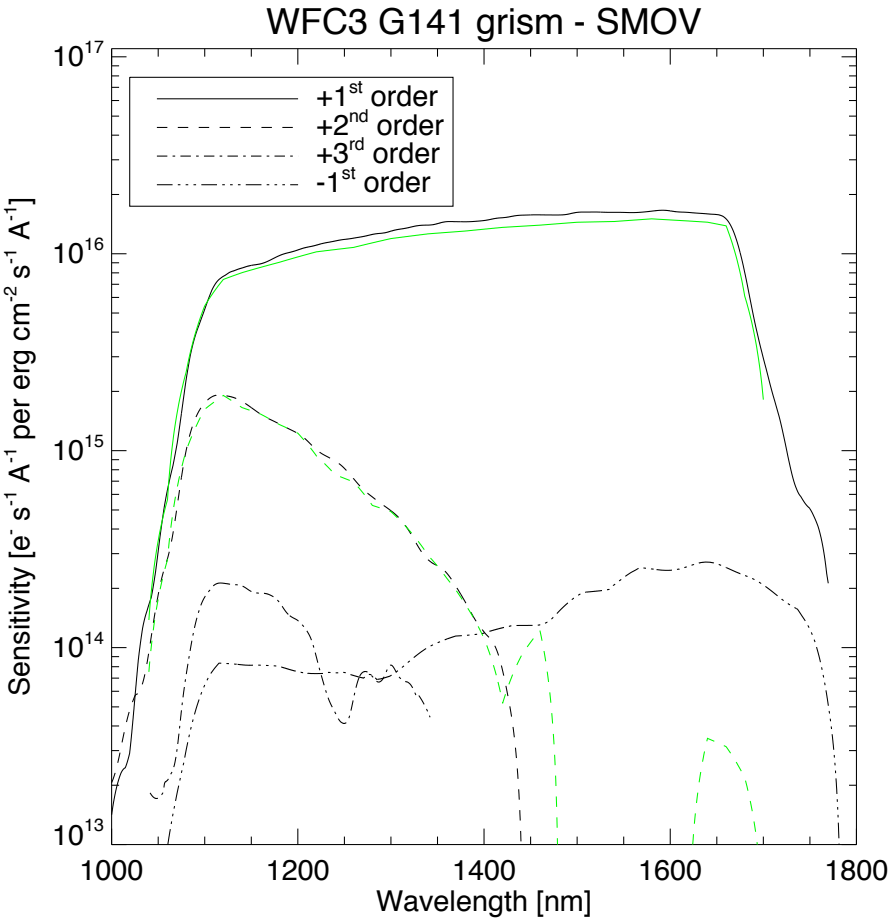

Figure 9: Sensitivities of the G141 grism for the +1st, +2nd, +3rd and -1st orders. The results were derived from the observations of the flux standard GD153 during SMOV (Proposal 11552). For comparison we show in green the measurements obtained during the TV3 ground calibrations.

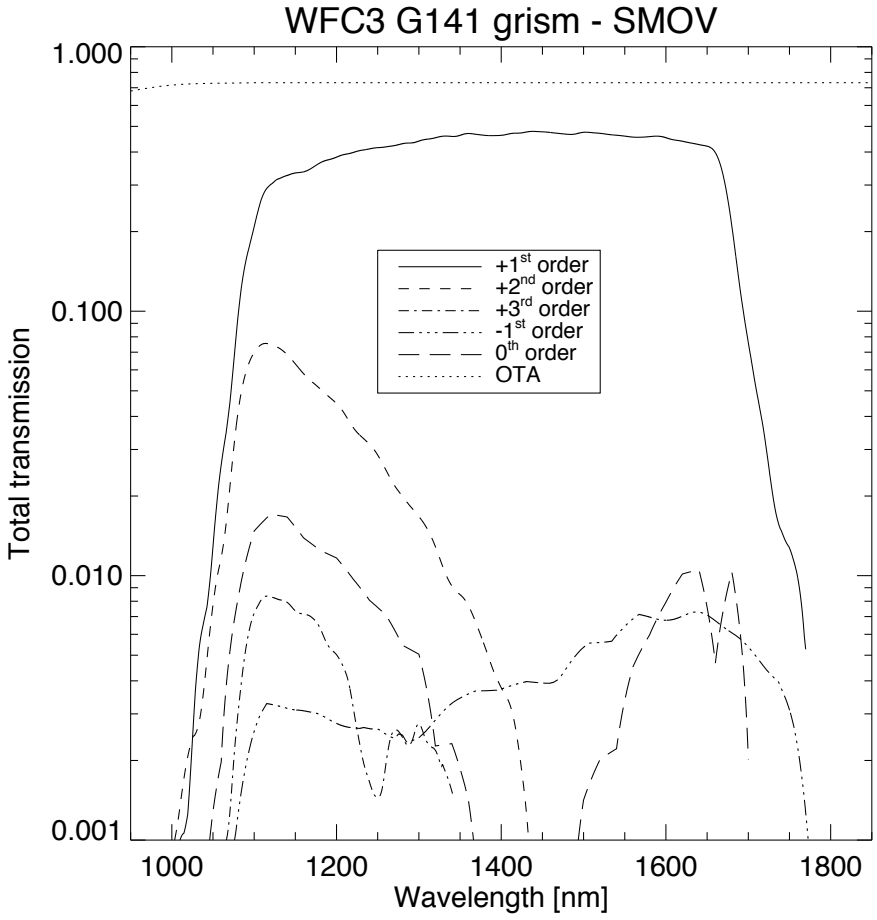

Figure 10: Total throughput estimates for the +1st, +2nd, +3rd and -1st orders of the G141 grism, derived from the sensitivity curves of this report. The 0th order is taken from the TV3 ground calibrations and only shown for comparison.

In Figure 11 we compare the total throughput estimates from the WFC3 IR grisms with "synphot" predictions. The synphot files are based and calibrated to WFC3 imaging from the SMOV observations. The plot shows theoretical values, which would be achieved with WFC3 without any filter or grism inserted. The analysis of the G141 grism is described in detail in Kuntschner et al. (2008a, b). The overall agreement to better than ±5% is good and shows that a consistent first order flux calibration of the IR channel was achieved.

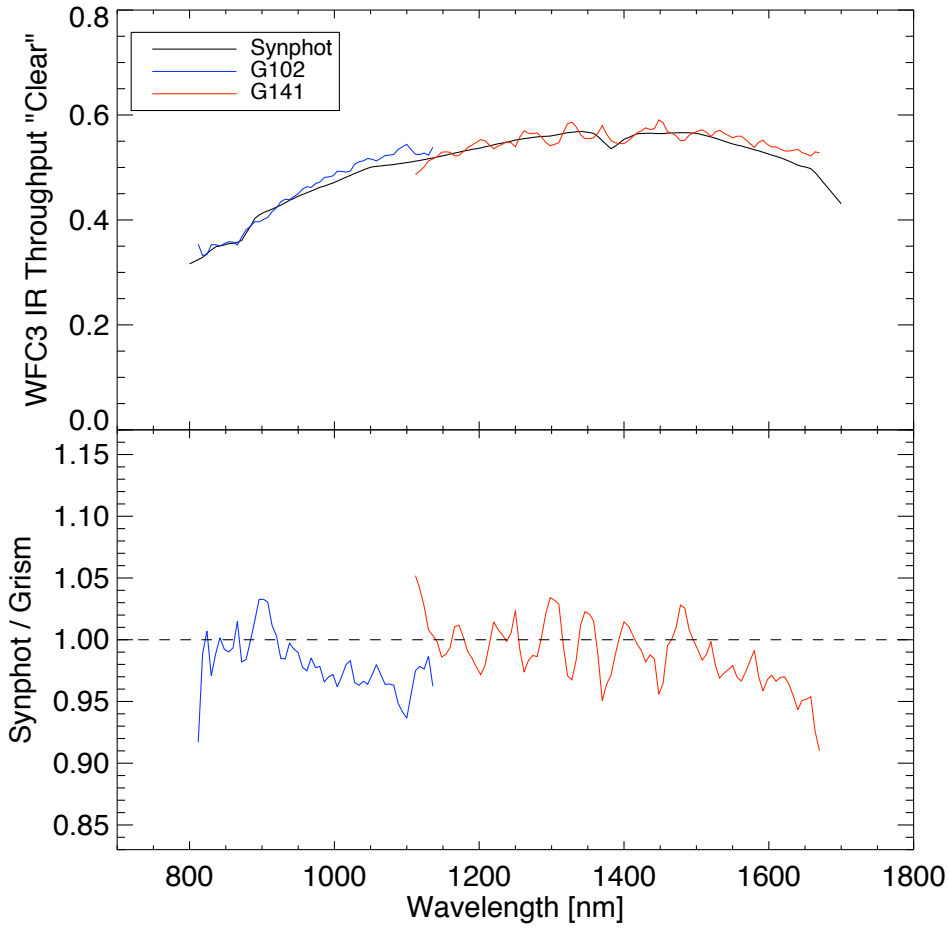

Figure 11: Comparison of total throughput "synphot" predictions with SMOV observations of the WFC3 IR grisms. The upper plot shows theoretical values, which would be achieved with WFC3 without any filter or grism inserted. The lower plot shows the ratio of "synphot" predictions over observations.

3.5. Aperture corrections and cross dispersion PSF

Using the aXe software (aXedrizzle option) we derived a rectified 2-dimensional image for the central exposures of the flux standard star GD153. The resulting image (called "stamp" image) is wavelength calibrated and image distortions, as recorded in our trace calibrations, are removed. From this image, covering a 220 pixel wide aperture around GD153, various sub-apertures (here used in the sense of

a diameter) are extracted with the help of IDL scripts and compared to the flu determined in the largest aperture. This procedure is carried out in five wavelength bins. The resulting aperture correction values are given in Tables 6 and shown in Figure 12. About 95% of the flux is concentrated in an aperture of 15 pixels diameter or 1.924 arcsec.

The aperture corrections derived from in orbit data compare well with TV3 results with a maximum difference of 4%.

Table 6: Aperture corrections for WFC3 G141

Diameter [arcsec]	11300 Å	12300 Å	13300 Å	14300 Å	15300 Å	16300 Å
0.128	0.445	0.442	0.402	0.347	0.345	0.375
0.385	0.811	0.791	0.770	0.750	0.741	0.724
0.641	0.892	0.875	0.871	0.866	0.861	0.850
0.898	0.918	0.899	0.899	0.897	0.895	0.889
1.154	0.939	0.922	0.920	0.916	0.914	0.904
1.411	0.953	0.937	0.937	0.934	0.932	0.922
1.667	0.963	0.947	0.948	0.947	0.946	0.936
1.924	0.971	0.956	0.957	0.956	0.956	0.946
3.719	0.991	0.982	0.986	0.988	0.991	0.977
7.567	0.997	0.992	0.996	0.998	1.001	0.991
12.954	0.999	0.995	0.999	1.001	1.002	0.994
25.779	1.000	1.000	1.000	1.000	1.000	1.000

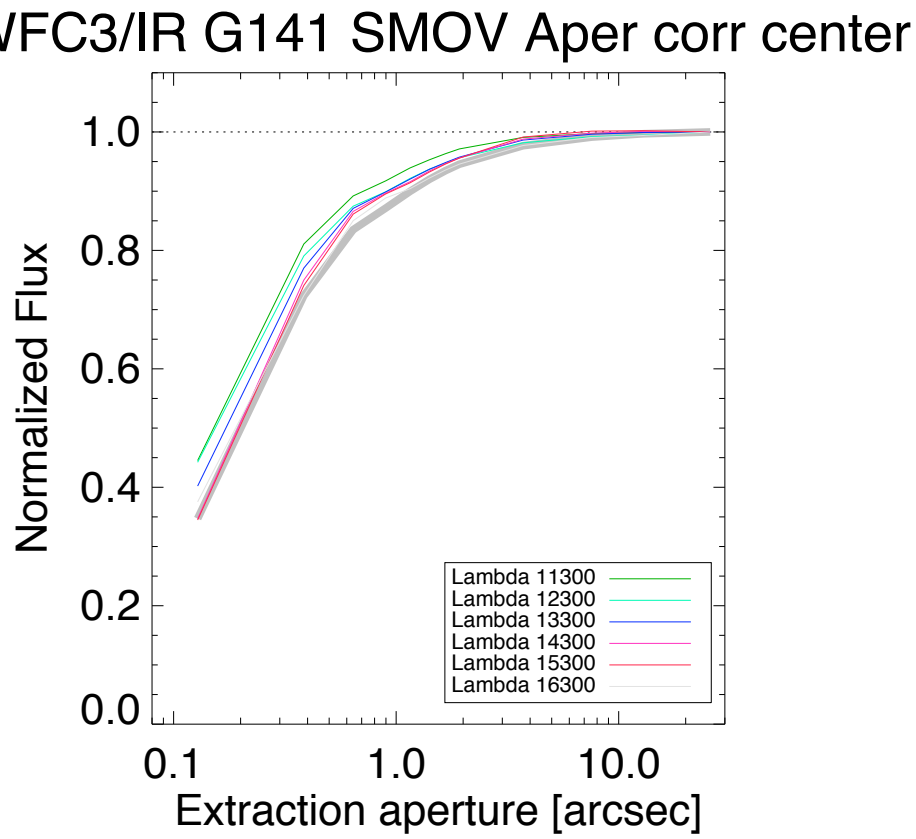

Figure 12: Aperture corrections for WFC3 G141 as a function of aperture (=diameter) and wavelength. For comparison TV3 data at 1330 nm is shown as thick grey line.

We also investigated the cross dispersion PSF of the central pointing for the flux standard star GD153. Ground calibration results showed that the G141 grism produces, for a Gaussian approximation, a cross dispersion width (FWHM) of XX to XX pixel (see Kuntschner et al. 2009). We show in Figure 13 the SMOV measurements, which indicate a slightly smaller width in comparison with TV3 results. Sampling effects cause the wave like structure of the measurements and we consider the minima as good representations of the true cross dispersion PSF. The measurements are also in agreement with the expectations from the direct imaging also shown in Figure 13. In conclusion, the G141 grism is in focus and produces spectra of point sources in agreement with design expectations.

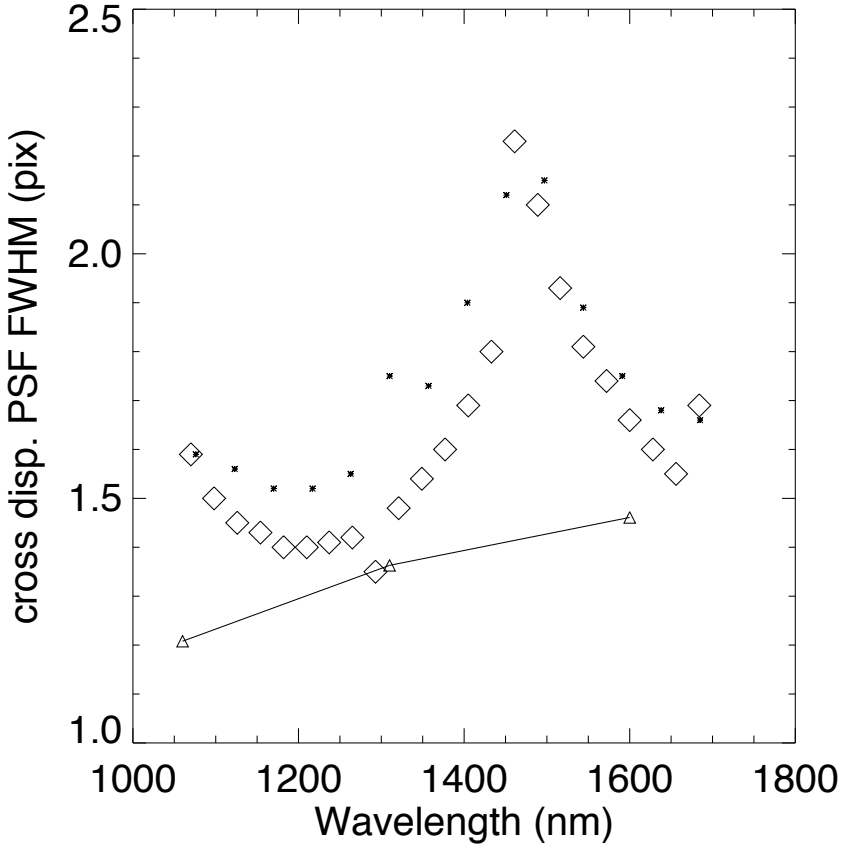

Figure 13: Cross-dispersion profile width as measured in FWHM (pixel) for a Gaussian approximation. Diamonds represent the SMOV data for one of the central pointings for grism G141. The small stars show estimates derived from white light images obtained during the TV3 ground calibrations (see Kuntschner et al. 2009). The triangles connected with a solid line show for comparison measurements from the TV3 direct light images as tabulated by Hartig (2008b).

4. Conclusions

This ISR presented the calibration of the WFC3 G141 grism based on SMOV data and one Cycle 17 wavelength calibration proposal. We have established in-orbit, source position dependent calibrations of the trace and wavelength solution for the $+1^{st}$ order "science" spectra. Both, the local trace and wavelength solution can be approximated with a linear solution. The mean dispersion of the G141 grism is

46.5 Å/pixel varying from 45.0 to 47.5 Å/pixel across the field of view. The in-orbit solutions agree well (<= 1 pixel) with the calibrations established during ground calibrations in TV2 and TV3. We also provide, field dependent calibrations for the $+2^{nd}$, $+3^{rd}$ and -1^{st} spectral orders, albeit with a less rigorous analysis.

We establish flux calibrations for the $+1^{st}$, $+2^{nd}$ $+3^{rd}$ and -1^{st} orders. Furthermore, we provide aperture corrections for the $+1^{st}$ order as a function of wavelength. The throughput of HST + WGC3 G141 peaks at 14350 Å with 47.8% and is above 10% between 10800 and 16900 Å.

Appendix

The datasets acquired during SMOV Proposal 11552 (PI Bushouse) and the Cycle 17 calibration program of Proposal 11937 (PI Bushouse) are listed in Table A1 and A2, respectively. Note, that throughout this report we use the name of "HB12" for the target PN G111.8-02.8.

Table A1. Summary of observations for the calibration of the grism G141 in Proposal 11552

FILE	TARGNAME	FILTER	EXPTIME [seconds]	POSTARG1 [arcsec]	POSTARG2 [arcsec]
iab904meq	GD-153	F140W	5.86	-20.0	0.0
iab904mfq	GD-153	F160W	5.86	-20.0	0.0
iab904mgq	GD-153	G141	102.93	-20.0	0.0
iab904mkq	GD-153	G141	102.93	-20.5	0.5
iab904mlq	GD-153	G141	102.93	-21.0	1.0
iab904mmq	GD-153	G141	202.93	-21.2	1.2
iab904moq	GD-153	F140W	5.86	23.0	-45.0
iab904mpq	GD-153	F160W	5.86	23.0	-45.0
iab904mqq	GD-153	G141	102.93	23.0	-45.0
iab9a4msq	GD-153	F140W	5.86	-50.0	45.0
iab9a4mtq	GD-153	F160W	5.86	-50.0	45.0
iab9a4muq	GD-153	G141	102.93	-50.0	45.0
iab908s3q	PN-G111.8-02.8	F140W	2.93	-20.0	0.0
iab908s4q	PN-G111.8-02.8	G141	102.93	-20.0	0.0
iab908s8q	PN-G111.8-02.8	F140W	2.93	-50.0	45.0
iab908s9q	PN-G111.8-02.8	G141	102.93	-50.0	45.0
iab908sdq	PN-G111.8-02.8	F140W	2.93	-20.0	45.0
iab908seq	PN-G111.8-02.8	G141	102.93	-20.0	45.0
iab908shq	PN-G111.8-02.8	F140W	2.93	23.0	45.0
iab908siq	PN-G111.8-02.8	G141	102.93	23.0	45.0

iab908slq	PN-G111.8-02.8	F140W	2.93	-50.0	0.0
iab908smq	PN-G111.8-02.8	G141	102.93	-50.0	0.0
iab908spq	PN-G111.8-02.8	F140W	2.93	23.0	0.0
iab908sqq	PN-G111.8-02.8	G141	102.93	23.0	0.0
iab908t9q	PN-G111.8-02.8	F140W	2.93	-50.0	-45.0
iab908taq	PN-G111.8-02.8	G141	102.93	-50.0	-45.0
iab908tdq	PN-G111.8-02.8	F140W	2.93	-20.0	-45.0
iab908teq	PN-G111.8-02.8	G141	102.93	-20.0	-45.0
iab908thq	PN-G111.8-02.8	F140W	2.93	23.0	-45.0
iab908tiq	PN-G111.8-02.8	G141	102.93	23.0	-45.0

Table A1. Summary of observations for the calibration of the grism G141 in Proposal 11937

FILE	TARGNAME	FILTER	EXPTIME [seconds]	POSTARG1 [arcsec]	POSTARG2 [arcsec]
ibbu02twq	VY2-2	F140W	5.86	-20.0	0.0
ibbu02txq	VY2-2	F160W	5.86	-20.0	0.0
ibbu02tyq	VY2-2	G141	102.93	-20.0	0.0
ibbu02tzq	VY2-2	G141	102.93	-20.5	0.5
ibbu02u0q	VY2-2	G141	102.93	-21.0	1.0
ibbu02u1q	VY2-2	G141	102.93	-21.2	1.2
ibbu02u3q	VY2-2	F140W	5.86	-50.0	45.0
ibbu02u4q	VY2-2	F160W	5.86	-50.0	45.0
ibbu02u5q	VY2-2	G141	102.93	-50.0	45.0
ibbu02uwq	VY2-2	F140W	5.86	-20.0	45.0
ibbu02uxq	VY2-2	F160W	5.86	-20.0	45.0
ibbu02uyq	VY2-2	G141	102.93	-20.0	45.0
ibbu02v0q	VY2-2	F140W	5.86	23.0	45.0
ibbu02v1q	VY2-2	F160W	5.86	23.0	45.0
ibbu02v2q	VY2-2	G141	102.93	23.0	45.0
ibbu02v3q	VY2-2	F140W	5.86	-50.0	0.0
ibbu02v4q	VY2-2	F160W	5.86	-50.0	0.0
ibbu02v5q	VY2-2	G141	102.93	-50.0	0.0
ibbu02v7q	VY2-2	F140W	5.86	23.0	0.0
ibbu02v8q	VY2-2	F160W	5.86	23.0	0.0
ibbu02v9q	VY2-2	G141	102.93	23.0	0.0
ibbu02vaq	VY2-2	F140W	5.86	-50.0	-45.0
ibbu02vbq	VY2-2	F160W	5.86	-50.0	-45.0
ibbu02vcq	VY2-2	G141	102.93	-50.0	-45.0
ibbu02veq	VY2-2	F140W	5.86	-20.0	-45.0
ibbu02vfq	VY2-2	F160W	5.86	-20.0	-45.0
ibbu02vgq	VY2-2	G141	102.93	-20.0	-45.0
ibbu02vhq	VY2-2	F140W	5.86	23.0	-45.0

ibbu02viq	VY2-2	F160W	5.86	23.0	-45.0
ibbu02vjq	VY2-2	G141	102.93	23.0	-45.0

References

Bertin, E., Arnouts, S. 1996, AAS, 117, 393

Cappellari M., Emsellem E., 2004, PASP, 116, 138

Hora, J. L., Latter, W.B., Deutsch, L. K., 1999, APJS, 124, 195

Kuntschner, H. Bushouse, H., Kümmel, M., Walsh, J. R., 2009, WFC3 Instrument Science Report, WFC3-2009-XX: The SMOV calibration of the WFC3 G102 grism

Kuntschner, H. Bushouse, H., Kümmel, M., Walsh, J. R., 2009, WFC3 Instrument Science Report, WFC3-2009-04: The cross dispersion profiles of the WFC3 grisms

Kuntschner, H. Bushouse, H., Walsh, J. R., Kümmel, M., 2008a, WFC3 Instrument Science Report, WFC3-2008-16: The TV3 ground calibrations of the WFC3 NIR grisms

Kuntschner, H. Bushouse, H., Walsh, J. R., Kümmel, M., 2008b, WFC3 Instrument Science Report, WFC3-2008-15: The TV2 ground calibrations of the WFC3 NIR grisms

Pirzkal, N., Bohlin, R. Thatte, D., 2009, NICMOS Instrument Science Report, NICMOS-2009-006: NICMOS Grism Wavelength Calibration